Eur. J. Mineral.
2016, **28**, 619–629
Published online 11 May 2016

Paper presented at the
8th European Conference on Mineralogy and Spectroscopy,
Rome, September 9–11, 2015

Crystal chemistry of "$Li_7La_3Zr_2O_{12}$" garnet doped with Al, Ga, and Fe: a short review on local structures as revealed by NMR and Mößbauer spectroscopy studies

DANIEL RETTENWANDER[1,*], REINHARD WAGNER[1], JULIA LANGER[2], MARIA ELISABETH MAIER[1], MARTIN WILKENING[2] and GEORG AMTHAUER[1]

[1] Department of Chemistry and Physics of Materials, University of Salzburg, Hellbrunnerstraße 34, 5020 Salzburg, Austria
*Corresponding author, e-mails: daniel.rettenwander@sbg.ac.at (Daniel Rettenwander); georg.amthauer@sbg.ac.at (Georg Amthauer)
[2] Christian Doppler Laboratory for Lithium Batteries, Institute for Chemistry and Technology of Materials, Graz University of Technology, Austria

Abstract: Cubic $Li_7La_3Zr_2O_{12}$ (LLZO) garnets stabilized by substitution of Li by supervalent cations (Al^{3+}, Ga^{3+} and Fe^{3+}) are exceptionally well suited to be used as protecting layer to enable Li-metal based battery concepts. On the one hand this dopants are needed to provide the outstanding properties of LLZO at room temperature (RT), but on the other hand dopants occupying Li sites are suspected to hinder the long-range Li-ion transport properties within the structure. This depends on the type of dopant species and their amount in the LLZO garnet. In particular, the way these dopants can be distributed in the garnet structure is thought to play a critical role in the Li-diffusion behaviour. This short review addresses the difficulty to obtain structural information on minor amounts of cations in a large complicated structure such as LLZO by diffraction methods and the advantages of the application of complementary spectroscopic methods, such as Mößbauer and NMR spectroscopy, which provide information on the valence state and the distribution of the dopants Al, Ga, and Fe over the possible cation positions of the garnet structure. Finally, (*i*) NMR spectroscopy at very high magnetic fields (21.1 T) shows that Al and Ga are similarly distributed over the 24*d* and 96*h* sites in the garnet structure and (*ii*) Mößbauer spectroscopy proves that Fe occurs in the trivalent state, also at the 24*d* and 96*h* sites of the cubic garnet framework. The solubility limit of Fe, Al, and Ga is up to 0.25 pfu, 0.39 pfu, and 0.72 pfu, respectively.

Key-words: LLZO garnet, ionic conductor, XRD, NMR spectroscopy, Mößbauer spectroscopy.

1. Introduction

Rechargeable Li-ion batteries are essential power sources for a large variety of portable electronic devices. Most Li-ion batteries now in use have liquid and polymer-supported electrolytes and they can have a number of unwanted, if not dangerous, properties such as dendrite formation, leakage and flammability. Thus, there is great current interest in finding and developing new solid-state fast Li-ion conductors that are thermally and chemically stable, paving the way for batteries with high energy densities. Recent research along these lines has shown that certain Li-oxide garnets have the necessary high ionic conductivities, as well as chemical and physical properties, to be considered as potential electrolytes in solid-state batteries (*e.g.* reviews of Cussen, 2010; Ramzy & Thangadurai, 2010; Zeier, 2014; Thangadurai *et al*., 2014).

"Garnet" is the common name for a large number of natural and synthetic metal oxide and fluoride phases. Conventional oxide garnets have the general formula $A_3B_2C_3O_{12}$ and crystallize in the cubic space group *Ia*-3*d* (Menzer, 1928). The O^{2-} ions in the general crystallographic positions 96*h* form an oxygen-atom framework with interstices occupied by the A cations, such as Ca^{2+}, Fe^{2+}, Y^{3+}, La^{3+} in the 8-fold coordinated position 24*c* (point symmetry 222), the B cations, such as Al^{3+}, Fe^{3+}, Zr^{4+}, Sn^{4+}, Sb^{5+}, *etc*. in the 6-fold coordinated position 16*a* (point symmetry −3), and the C cations, such as Li^{+}, Al^{3+}, Fe^{3+}, Ga^{3+}, Ti^{4+}, Si^{4+}, *etc*. in the 4-fold coordinated 24*d* position (point symmetry −4). In addition to these cation sites, there are other interstices within the oxygen framework, which are empty in the conventional garnet structure, *e.g.*, (i) the 6-fold coordinated 16*b* positions with point symmetry 32, (ii) the 6-fold coordinated 48*g* positions with point symmetry 2, and (iii) an additional 4-fold coordinated 96*h* position with point symmetry 1 (Hellner *et al*., 1979). These interstices or voids can be filled by "excess" cations such as Li^{+} or H^{+} and by this enable ionic conductivity.

Among the Li-bearing garnet group, $Li_7La_3Zr_2O_{12}$ (LLZO) has one of the highest Li-ion conductivities

DOI: 10.1127/ejm/2016/0028-2543 0935-1221/16/0028-2543 $ 4.95

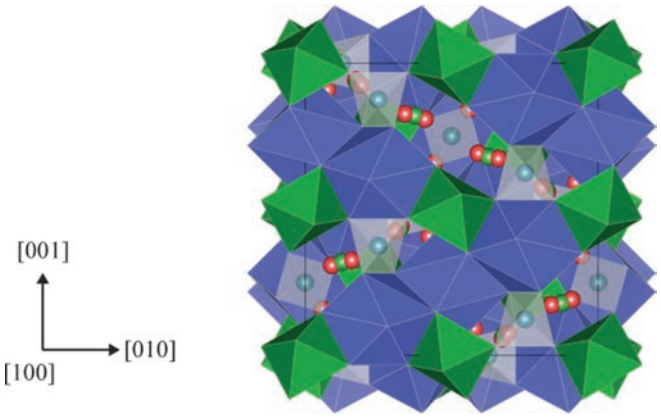

Fig. 1. Crystal structure of cubic $Li_7La_3Zr_2O_{12}$ (*Ia*-3*d*). Blue dodecahedra are occupied by La^{3+} (24*c*), green octahedra by Zr^{4+} (16*a*). Li^+ is distributed over three sites: (i) tetrahedrally coordinated (24*d*) sites represented by light blue spheres; (ii) octahedrally coordinated (48*g*) sites represented by green spheres, and (iii) distorted four-fold coordinated (96*h*) sites represented by red spheres. (Online version in colour)

measured to date for any crystalline phase (Murugan *et al*., 2007). Research indicates that pure LLZO is tetragonal (space group $I4_1/acd$) at room temperature (RT) with a significantly lower ionic conductivity of about 10^{-6} S cm^{-1} than that of the high-temperature cubic phase (space group *Ia*-3*d*) that has an ionic conductivity of about 10^{-3}–10^{-4} S cm^{-1} at RT (Murugan *et al*., 2007; Awaka *et al*., 2009; Kuhn *et al*., 2011). Fortunately, the cubic modification can be easily stabilized at RT by supervalent dopants, *e.g.*, Al^{3+}, Ga^{3+}, and Fe^{3+}. These dopants are needed to provide the exceptional properties LLZO at RT, but dopants occupying Li sites are suspected to hinder the long-range Li-ion transport properties within the structure. This depends on the type of dopant species and its amount in the LLZO garnet. In particular, the way these dopants can be distributed over the three possible crystallographic sites containing Li in the garnet structure (Fig. 1) is thought to play a critical role in the Li-diffusion behaviour.

Because of the importance of aliovalent cation substitution for the stabilization of the highly conducting cubic LLZO phase, long-range (*e.g.*, X-ray, and neutron diffraction) as well as short-range methods (*e.g.*, NMR, and ^{57}Fe Mößbauer spectroscopy) were intensively applied to locate the dopants in the cubic LLZO structure. This short review is mainly based on the papers of Rettenwander *et al*. (2015a and b) and gives an overview about the state of research. Because of the difficulty to obtain structural information on minor amounts of cations in a large complicated structure as LLZO by diffraction methods, this paper focusses on the application of spectroscopic methods, such as Mößbauer and NMR spectroscopy, which provide information on the valence state and the distribution of the dopants Al, Ga, and Fe over the possible cation positions of the garnet structure.

2 Experimental methods

2.1 Synthesis

A series of Li_{7-3x} M_x^{3+} $La_3Zr_2O_{12}$ garnets with $M = Al^{3+}$, Ga^{3+}, and Fe^{3+} and with intended mole fractions of M (x_{int}) with up to $x_{int} = 1.00$ per formula unit (pfu) was synthesized by high-temperature sintering methods. The starting materials were Li_2CO_3 (99 %, Merck), La_2O_3 (99.0 %, Aldrich), ZrO_2 (99.0 %, Aldrich) Al_2O_3 (99.0 %, Aldrich), Ga_2O_3 (99.0 %, Aldrich), and ^{57}Fe enriched Fe_2O_3. The latter was used to obtain well resolved ^{57}Fe Mößbauer spectra (see below). Li_2CO_3 was mixed with the various oxides in the necessary proportions and they were ground intimately together. This mixture was calcined at 900°C, reground, pressed into pellets, and sintered at 1050°C for 16 h and then removed from the furnace to cool down. To avoid Li evaporation and undesired contamination from the corundum crucible, the pellets were arranged between pellets of pure LLZO.

For SEM analysis, polycrystalline chips from the pellets were embedded in epoxy holders, the surface was ground and then polished using diamond paste.

2.2 X-ray powder diffraction (XRPD)

A small fragment taken from the middle of a sintered polycrystalline pellet was ground and used for X-ray powder diffraction. The XRPD patterns were collected using a Siemens D8 diffractometer with Cu*K*α radiation. Data were collected between 10° and 70° 2θ. The garnet lattice parameter, a_0, and grain size were determined by Rietveld refinement using the program Topas V2.1 (Bruker AXS). All the ionic radii reported in this paper are taken from Shannon & Prewitt (1969).

2.3 Electron probe micro-analysis (EPMA)

Quantitative chemical analyses were done using a JEOL 8100 SUPERPROBE at the University of Innsbruck. Small polycrystalline chips, taken from the larger pellets, were embedded in an epoxy holder and the surface was ground and then polished using diamond paste. For the analysis, special attention was paid to grain sizes, grain boundaries and textures. Analytical measuring conditions were 15 kV accelerating voltage and a 10 nA beam current. The standards used were synthetic almandine, $Fe_3Al_2Si_3O_{12}$, for Fe, synthetic La-phosphate, LaP_5O_{14}, for La, and synthetic zircon, $ZrSiO_4$, for Zr. Measuring times were 20 s for the peak maximum and 10 s for the background. Wavelength-dispersive spectroscopy (WDS) measurements were made to characterize the synthetic products in terms of their chemical homogeneity for the elements La, Zr, and Fe. Twenty point measurements, distributed over five different grains, were made and combined to obtain a representative composition for a given synthesis product.

2.4 Inductively coupled plasma optical emission spectroscopy (ICP-OES)

Measurements were made with a Horiba Jobin Yvon Ultima 2 device at the University of Ulm to determine the Li contents. About 50 mg taken from the sintered pellet were divided into two batches in order to test the analytical reproducibility. The samples were prepared by dissolving 15 mg of garnet in 2 ml of *aqua regia* (HCl + HNO_3) followed by heating to complete dissolution of the garnet. Deionized water was then added to obtain 20 ml of solution. Finally, 1 ml aliquots were taken for the ICP-OES measurements.

2.5 ^{57}Fe Mößbauer spectroscopy

Spectra were recorded using a multichannel analyzer (1024 channels) operating in conjunction with an electromechanical drive system with symmetric triangular velocity shape. The two simultaneously obtained spectra (512 channels each) were folded and evaluated assuming Lorentzian line shapes, as well as quadrupole splitting distributions, QSDs, using the program Recoil (Lagarec & Rancourt, 1998). During the measurement, the source (^{57}Co/Rh, 50 mCi) and absorber were kept at room temperature. Isomer shift values are reported relative to α-iron at RT.

2.6 NMR spectroscopy

2.6.1 Low-field ^{71}Ga MAS NMR

Spectra were recorded at room temperature on the same Ga^{3+} doped samples which were characterized by XRPD, EPMA, and ICP-OES using a Bruker ASX 400 spectrometer at Ruhr University of Bochum. The spectra were collected at 122 MHz (9.4 T) with a spinning rate of 12.5 kHz using 4 mm MAS probe. The ^{71}Ga MAS NMR experiments consisted of single pulse duration of 0.6 μs with a delay time after each pulse of 8 μs with a spectral width of 125 kHz corresponding to a solid radio-frequency tip angle of about 15° ± 5. Signal to noise ratio was optimized by a pulse delay of 0.4 μs and using full relaxation for short pulses. A line broadening of 100 Hz was applied and the first four to eight points of 1000 measured FID points had to be removed because of strong distortion and low signal. The count of the spectral points was 8000. The lineshape was simulated using the STARS simulation package in VNMR [26]. The ^{71}Ga chemical shifts are reported relative aqueous 1 M $Ga(NO_3)_3$.

2.6.2 High-field ^{71}Ga MAS NMR

Spectra, including the (multiple quantum) MQMAS spectra, were acquired at RT using a high-performance Bruker Advance II 900-MHz spectrometer. The spectrometer is connected to a cryomagnet with a nominal field of 21.1 T; it is installed at the National Ultrahigh-Field NMR facility in Ottawa; 21.1 T correspond to Larmor frequencies $\omega_0/2\pi$ of 234.5 MHz for ^{27}Al und 274.5 MHz for ^{71}Ga, respectively. All experiments were performed under MAS conditions at spinning rates of 25 kHz (^{27}Al), 31.25 kHz (^{27}Al MQMAS) and 30 kHz (^{71}Ga), respectively, using Bruker 2.5 mm H/X probes. Chemical shift values, δ_{iso}, were referenced to 1M aqueous solutions of $Al(NO_3)_3$ and $Ga(NO_3)_3$, respectively. The spectra were recorded via single pulse excitation; pulse lengths of 1.0 μs (^{27}Al) and 0.5 μs (^{71}Ga) were used. For the ^{27}Al and ^{71}Ga measurements the recycle delays were set to 0.5 s and 5 s, respectively. The ^{27}Al spectra were typically recorded with 640 scans (samples with the compositions $Ga_{0.0}Al_{0.4}$, $Ga_{0.1}Al_{0.3}$, and $Ga_{0.2}Al_{02}$) and 11k scans ($Ga_{0.3}Al_{0.1}$). The ^{71}Ga spectra were acquired with 16k scans ($Ga_{0.4}Al_{0.0}$, $Ga_{0.3}Al_{0.1}$, $Ga_{0.2}Al_{0.2}$) or 32k scans ($Ga_{0.1}Al_{0.3}$). The DMFit software was used to simulate the line shapes and to determine chemical shift values as well as to estimate the corresponding coupling constants and asymmetry parameters.

3 Results

For the sake of simplicity, sample formulae are given as follows:

$$Li_{7-3x}Fe_xLa_3Zr_2O_{12} \rightarrow LLZO:Fe_x$$
$$Li_{7-3x}Fe_xLa_3Zr_2O_{12} \rightarrow LLZO:Ga_x$$
$$Li_{7-3(x+y)}Ga_{x-y}Al_yLa_3Zr_2O_{12} \rightarrow LLZO:Ga_xAl_x$$

Furthermore, x_{int} is the intended, x_{obs} the observed/measured mole fraction of the relevant cation.

3.1 $Li_{7-3x}Fe_x^{3+}La_3Zr_2O_{12}$ (LLZO:Fe_x)

The incorporation of the transition element Fe into the Li-oxide garnet structure at the Li^+ positions was first reported by Rettenwander *et al*. (2013, 2015a). Their results will be reviewed in the following. The knowledge of the oxidation state of Fe as well as of the lattice positions occupied by Fe is of great interest in order to understand a possible influence on the ionic conductivity.

3.1.1 Phase identification and chemical characterization

A series of LLZO:Fe_x with x_{int} = 0.04–0.72 per formula unit (pfu) was synthesized by high-temperature sintering methods as reported above. The XRPD pattern of a typically LLZO:Fe_x is shown in Fig. 2, together with the patterns of cubic and tetragonal LLZO from Awaka *et al*. (2009) and Han *et al*. (2012).

Single-phase cubic LLZO garnet could be synthesized for compositions with $0.08 < x_{int} < 0.52$. Only one weak reflection that does not match the cubic pattern was observed for the sample with x_{int} = 0.52, and it could be assigned to $FeLaO_3$ (about 0.5 wt%). This indicates that the maximum solubility limit is below 0.52 Fe pfu. The

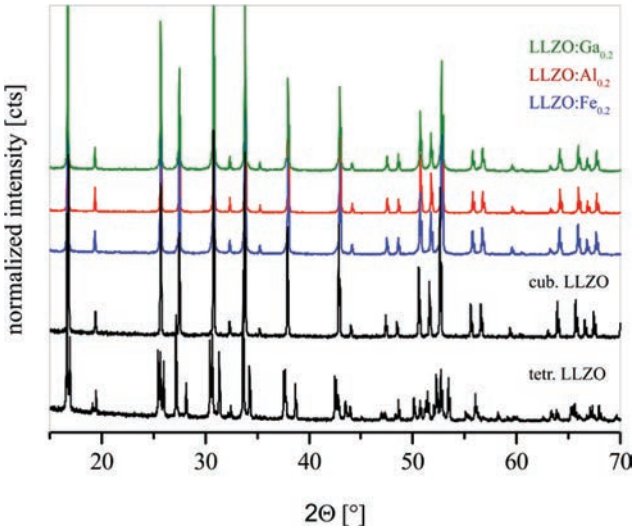

Fig. 2. X-ray powder diffraction pattern of cubic LLZO:$Fe_{0.16}$, LLZO:$Al_{0.40}$, and LLZO:$Ga_{0.40}$ (*Ia*-3*d*), together with the patterns of cubic and tetragonal LLZO from Awaka *et al*. (2009) and Han *et al*. (2012). The XRPD pattern of the whole solid solutions can be found in Rettenwander *et al*. (2013, 2014a and b, 2015a and b). (Online version in colour)

lattice constant a_0 of all solid-solution cubic garnets is similar within the experimental error and was determined to be a_0 = 12.980(5) Å regardless of the amount of Fe^{3+}.

The chemical analyses obtained using electron microprobe and ICP-OES measurements and the calculated mole fractions of all elements in LLZO:Fe_x with intended mole fraction of Fe x_{int} = 0.04–0.72 show that, in all the samples, the measured Fe values x_{obs} are distinctly lower than the intended stoichiometric amount x_{int} of Fe. The upper solid-solution limit for Fe in LLZO therefore appears in agreement with the Mößbauer results to be about x_{obs} = 0.25 measured in the sample with x_{int} = 0.64. The crystal chemical formulae for $Li_{7-3x}Fe_xLa_3Zr_2O_{12}$ with x_{int} = 0.04–0.24 are:

$$x_{int} = 0.04 : Li_{6.89}Fe_{0.03}La_{3.05}Zr_{2.01}O_{12},$$
$$x_{int} = 0.08 : Li_{6.66}Fe_{0.06}La_{3.06}Zr_{2.01}O_{12},$$
$$x_{int} = 0.16 : Li_{6.54}Fe_{0.12}La_{3.01}Zr_{1.98}O_{12}, \text{and}$$
$$x_{int} = 0.24 : Li_{6.19}Fe_{0.19}La_{3.02}Zr_{2.04}O_{12}.$$

Formulae for LLZO:Fe_x with x_{int} > 0.24 are not given, because the exact Li content of these samples was not measurable due to the presence of extra phases in the synthetic products.

3.1.2 Site distribution of Fe (^{57}Fe Mößbauer spectroscopy)

The ^{57}Fe Mößbauer spectrum of LLZO:Fe_x with x_{int} = 0.16 (x_{obs} = 0.12) taken at RT is displayed in Fig. 3a. The spectrum exhibits two resonant absorption lines which can be evaluated by two quadrupole doublets. After several attempts, it became clear that it was not possible to obtain a satisfactory fit of the spectrum using quadrupole split doublets having simple Lorentzian line shapes. Therefore, two quadrupole splitting distributions assuming Voigt line shapes were used applying the fit program Recoil of Lagarec & Rancourt (1998). The fit gives a

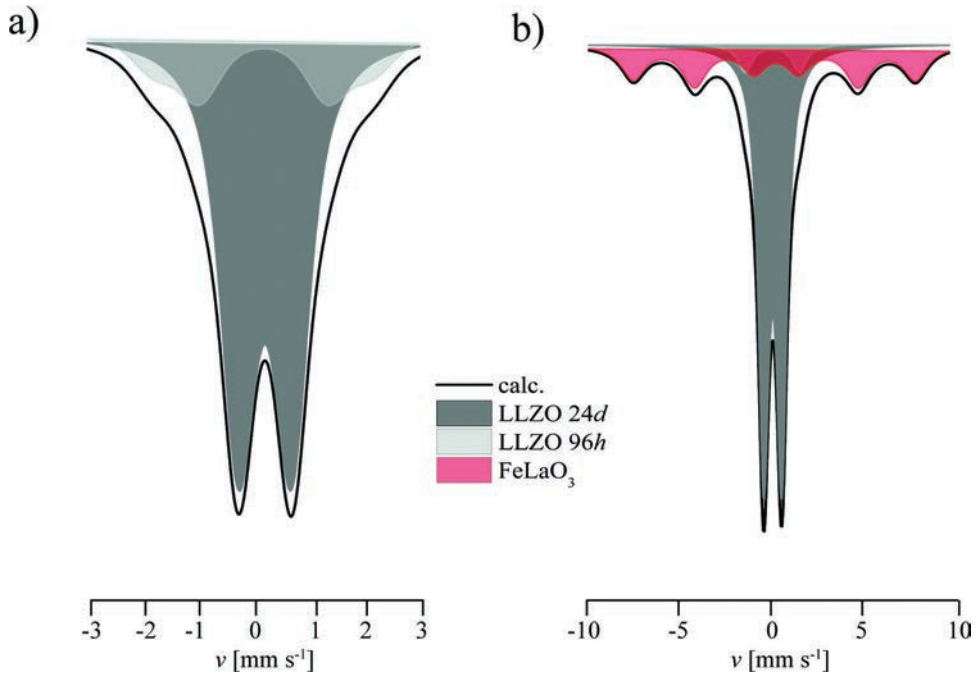

Fig. 3. (a) ^{57}Fe Mößbauer spectrum of ^{57}Fe-bearing $Li_{7-3x}Fe_x^{3+}La_3Zr_2O_{12}$ garnet with x_{int} = 0.16 (x_{obs} = 0.12) taken at RT. (b) ^{57}Mößbauer spectrum of $Li_{7-3x}Fe_x^{3+}La_3Zr_2O_{12}$ garnet with x_{int} = 0.44 (x_{obs} = 0.17) (from Rettenwander *et al*. 2015a). (Online version in colour)

reasonable χ^2 value of 1.56. On the basis of their different isomer shift, δ, and quadrupole splitting, $\Delta E_{Q,}$ values, they are assigned to Fe^{3+} located at two different structural sites in LLZO. The most intense Fe^{3+} doublet with an area, A, of 79 % has an isomer shift $\delta = 0.20$ mm/s and a quadrupole splitting of $\Delta E_Q = 0.96$ mm/s. These values are similar to the isomer shift and quadrupole splitting values of Fe^{3+} at the 24*d* tetrahedral position in natural and synthetic garnets ($Y_3(Fe,Ga)_5O_{12}$), *i.e.*, $\delta = 0.20$ mm/s and $\Delta E_Q = 0.98$ mm/s (Amthauer *et al*., 1986; Nitsche *et al*., 1994). Therefore, this doublet in the spectrum of Fe-bearing LLZO is assigned to Fe^{3+} at the 24*d* site.

The second most intense Fe^{3+} quadrupole doublet, with an area of 21 % of the total resonant absorption, results from a superposition of two components with an identical isomer shift value of $\delta = 0.18$ mm/s but with different quadrupole splitting values of $\Delta E_Q = 2.30$ mm/s and 3.95 mm/s, respectively. Together the two components have a combined quadrupole splitting value of $\Delta E_Q = 2.87$ mm/s. The isomer shift $\delta = 0.18$ mm/s indicates tetrahedrally coordinated Fe^{3+}. The large quadrupole splitting values of both components indicate strongly distorted oxygen coordination polyhedra. The question is how both components can be interpreted. In the case of Al-bearing LLZO, the Al^{3+} cation can be displaced from the centre of the special crystallographic site 48*g* to an off-centered general 96*h* position. The displacement of Al^{3+} from 48*g* depends on the various local site occupations of Al^{3+} (Rettenwander *et al*., 2014a) The situation with Fe^{3+} can be expected to be similar. Thus a range of different local coordination polyhedra around Fe^{3+} arises and this gives rise to an asymmetric and broad line shape. Therefore, this second complex doublet is assigned to Fe^{3+} in various locally distorted polyhedral coordinations around 96*h* positions resulting in a distribution of different electric field gradients and a quadrupole splitting distribution.

We did not detect any Fe^{2+} in the garnets studied here, as reported in our previous study (Rettenwander *et al*., 2013).

An additional six-line resonant absorption pattern appears in the spectra of the samples with Fe contents higher than $x_{int} = 0.24$, 0.36 and 0.44, indicating an additional phase with magnetic hyperfine interaction (Fig. 3b). The paramagnetic subpattern was evaluated using similar hyperfine parameters as those evaluated for the sample with $x_{int} = 0.16$. These parameters were kept constant during the fitting procedure of the magnetic subpattern. This approach is the best approximation of the situation even though χ^2 became rather large with a value of 13.7. The evaluation of this additional magnetic subpattern gives an isomer shift of $\delta = 0.36$ mm/s, a quadrupole splitting of $\Delta E_Q = 0.04$ mm/s, a magnetic hyperfine field of $H_{HF} = 484$ kOe, and an area of $A_3 = 34\%$ of the total resonant absorption area in the spectrum of the sample $x_{int} = 0.44$ ($x_{obs} = 0.17$). These parameters agree well with those of nano-crystalline $FeLaO_3$ reported in the literature; therefore, we assigned this magnetic hyperfine pattern tentatively to the phase $FeLaO_3$ (Sivakumar *et al*., 2004), which also appears in XRPD of the same sample.

3.2 $Li_{7-3(x+y)}Ga_{x-y}Al_yLa_3Zr_2O_{12}$, (LLZO:$Ga_xAl_y$)

Much experimental as well as theoretical effort has been undertaken to collect information on the local coordination and the site preferences of the dopants Al and Ga in LLZO. Rettenwander *et al*. (2014a) have shown on the basis of a DFT study that Al preferentially occupies the tetrahedrally coordinated 24*d* sites as well as the distorted four-fold coordinated 96*h* sites in LLZO. For Ga, on the other hand, recent NMR studies indicated that only a single site (*viz.* the 96*h* site) is occupied by the dopant, irrespective of the amount of Ga introduced (Rettenwander *et al*., 2014b). Since the 24*d* site forms a junction between the loops of the Li-ion pathways in LLZO, the occupation of this site is suspected to act as a blockade for the mobile Li ions; this might be in contrast to the situation when only the 96*h* sites are occupied (see Fig. 1). Consequently, provided there is a significantly different site preference of Al and Ga, respectively, one might expect a measurable influence on Li-ion transport properties of LLZO as discussed by Allen *et al*. (2012).

3.2.1 Sample description

In order to prove this assumption, we synthesized mixed-doped LLZO:Ga_xAl_y with varying portions of Al and Ga was synthesized. Here, a series with intended mole fractions, x, $y \in \{0.0, 0.1, \ldots, 0.8\}$ and $x + y \leq 0.8$ were synthesized by conventional high-temperature sintering method similar to LLZO:Fe_x (Rettenwander *et al*., 2013)

As an example the solid-solution series LLZO:$Ga0_{.4-y}Al_y$ is presented and discussed in detail in this review. For the results of all other solid solutions, the reader is referred to Rettenwander *et al*., (2015b) and its Supplemental Materials Section.

The XRPD patterns of the $Ga_{0.4-y}Al_y$ exhibit reflections clearly showing cubic symmetry (Fig. 2). There are no indications of any phases formed other than cubic LLZO for $Ga_{0.4-y}Al_y$ with $y < 0.4$. The sample with $y = 0.4$ shows a low-intensity, but single reflection representing <1 wt% $LaAlO_3$. This impurity phase is also seen by NMR in the sample with $y = 0.3$; in that case it seems to be X-ray amorphous. The other samples are single phase, regardless of the intended portion of dopants. In all solid solutions with $x + y > 0.5$ the number and the amount of extra phases increase with the portion of Al. Typically, these extra phases are $LaAlO_3$, Li_2ZrO_3 and $La_2Zr_2O_7$; the more Al is present the more easily those phases are formed. The evaluation of the LLZO portion in the syntheses gives evidence for a lower incorporation limit of Al as compared to Ga. Phase pure Ga-doped LLZO can be synthesized up to $x = 0.8$; this is in contrast to pure Al-doped LLZO for which the incorporation limit turns out to be approximately 0.3 pfu.

The unit-cell constant, a_0, was evaluated by Rietveld analysis. There is no indication for a_0 to follow a general trend for the single-doped solid solutions (Ga_xAl_0, and Ga_0Al_y). Our findings are in accordance with previous studies on Ga-doped LLZO where the lattice parameter a_0 does not change systematically or significantly with the amount of dopants. This is probably related to the aliovalent doping mechanism, where 3 Li^+ are substituted by 1 Ga^{3+}, and to the variation in site occupation. Interestingly, the a_0 value increases with the Ga portion by approximately 0.015 Å / Ga pfu. Here in our study the Li content remains constant but Al is continuously replaced by Ga within one series. So in this case the larger ionic radius of Ga seems to be responsible for the slight increase of a_0 observed.

3.2.2 *^{27}Al and ^{71}Ga NMR*

The nuclei ^{71}Ga (I = 3/2 (see above), natural abundance 39.6 %) and ^{27}Al (I = 5/2, natural abundance 100.0 %) are quadrupolar; the corresponding interaction of their quadrupole moments (Q_{Ga} = 1.07 × 10^{-29} m^2 and Q_{Al} = 1.616 × 10^{-30} m^2) with surrounding electric-field gradients results in specific shapes of the NMR lines that depends on the interplay of the magnitude of the external magnetic field applied and the underlying coupling constant and asymmetry parameters characterizing the interaction. While first-order electric quadrupole interactions are largely eliminated by sufficiently fast spinning, MAS is unable to remove the second-order effects. Selected NMR spectra of samples with the composition LLZO:$Ga_{0.40-y}Al_y$ with y = 0.4 and y = 0.0 are shown in Figs 4 and 5, respectively.

The ^{27}Al NMR spectra of Al-doped LLZO have already been extensively analysed in the past (Fig. 4, upper part). In accordance with previous reports our ^{27}Al spectrum of mixed LLZO:Ga_xAl_y (Fig. 4, lower part) shows, irrespective of the amount of Al inserted, two characteristic resonances with δ_{iso} of *ca*. 66 ppm and *ca*. 81 ppm. For the samples with high Al content an additional resonance at δ_{iso} = 12 ppm was found; it reflects octahedrally coordinated Al^{3+} ions in $LaAlO_3$, which is a known extra phase that forms during the synthesis of Al-doped LLZO (Buschmann *et al*., 2011). As mentioned above, $LaAlO_3$ was also observed by XRPD for samples with high Al content. Since in our case the magnetic field interaction at B_0 = 21.1 T is much stronger compared to the quadrupole interactions, the high-field ^{27}Al spectra largely benefit from a better resolution. Fortunately, this results in sharp signals with almost isotropic line shapes. For this reason, the ^{27}Al NMR parameters C_Q and η_Q cannot be simulated well with DMFit. The chemical shift values, however, can be precisely read off; they fit almost perfectly with the NMR parameters of Rettenwander *et al*. (2014a) recently calculated by DFT methods. Furthermore, on the basis of their DFT study, Rettenwander *et al*. (2014a) assign the resonances with chemical shifts δ_{iso} close to 66 ppm and 81 ppm to Al ions residing on the 24*d* and 96*h* sites, respectively.

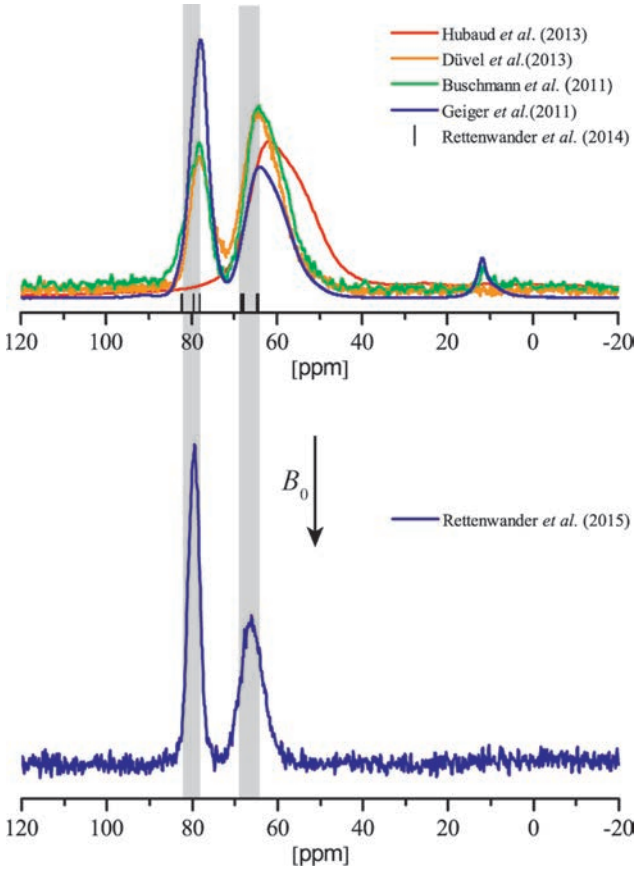

Fig. 4. Top: ^{27}Al MAS NMR spectra reported from literature measured at low field B_0 = 9.4 T. See text for further details. Bottom: ^{27}Al MAS NMR spectrum of $Li_{5.8}Ga_{0.00}Al_{0.40}La_3Zr_2O_{12}$ garnet measured at high field B_0 = 21.1 T. (Online version in colour)

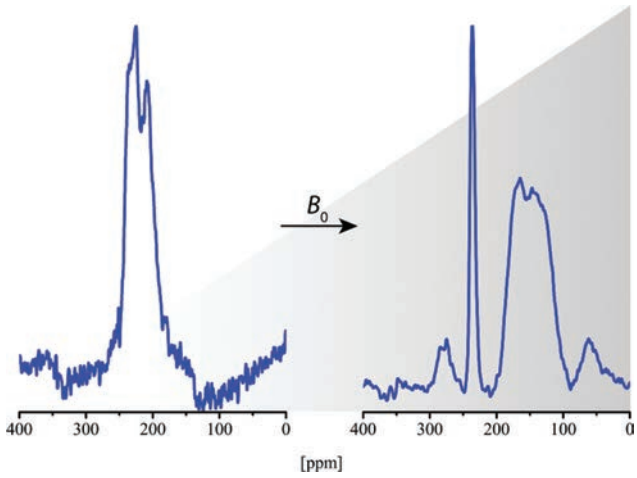

Fig. 5. MAS NMR spectra of ^{71}Ga in $Li_{5.8}Ga_{0.40}Al_{0.00}La_3Zr_2O_{12}$ garnet recorded at B_0 = 9.4 T (left) and at B_0 = 21.1 T (right). See text for further details. (Online version in colour)

This assignment is in agreement with almost all experimental studies of other groups that focus on the site preference of Al in LLZO; the resonance near 66 ppm has consistently been interpreted to reflect Al^{3+} ions on the 24*d* position (Buschmann *et al*., 2011; Geiger *et al*.,

2011; Düvel *et al*., 2012). In all of the three previous studies, a second resonance shows up in the ^{27}Al MAS NMR spectra of LLZO:Al at approximately 80 ppm. It can be assigned to the distorted four-fold coordinated 96*h* position. Because of the asymmetric line shape of this resonance the signal was suspected to be a superposition of more than one NMR line showing up in the region from 75 to 85 ppm. These results were afterwards confirmed and reinterpreted using DFT methods (Rettenwander *et al*., 2014a).

In contrast to these three studies, Hubaud *et al*. (2013) report only one resonance at about 60 ppm which is extraordinarily broad and, therefore, interpreted by the authors as a superposition of two lines assigned to two different 24*d* sites in at least two different LLZO phases, which have not yet reached the thermodynamic equilibrium.

In order to resolve potentially overlapping lines Rettenwander *et al*. (2015b) studied $Ga_{0.2}Al_{0.2}$ and $Ga_{0.0}Al_{0.4}$ with the help of MQMAS NMR (Fig. 6).

The ^{27}Al 3QMAS spectra of $Ga_{0.2}Al_{0.2}$ and $Ga_{0.0}Al_{0.4}$ essentially prove that the line broadening is not caused by distinct overlapping sites. However, it is worth noting that the diagonal streaking in the 2D projection indicates a certain distribution of chemical shifts reflecting a small amount of disorder or strain in the sample. This feature is even more pronounced in the ^{27}Al 3QMAS spectrum of $Ga_{0.0}Al_{0.4}$ for the resonance at 81 ppm reflecting the distorted 96*h* site (see Fig. 6). Thus, in agreement with previous works, the two signals observed reflect Al^{3+} ions clearly residing on only two distinct sites, *viz.* the magnetically inequivalent 24*d* and 96*h* voids, respectively.

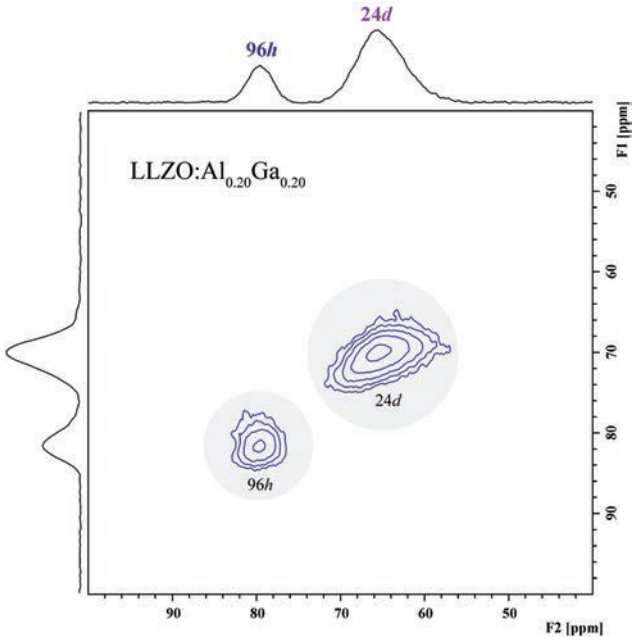

Fig. 6. The 3Q MAS spectra of $Ga_{0.2}Al_{0.2}$ and $Ga_{0.0}Al_{0.4}$ recorded at 21.1 T and a spinning speed of 31.25 kHz (taken from Rettenwander *et al*. 2015b). (Online version in colour)

Assignments for the ^{71}Ga NMR peaks are not as well established in the literature as the ^{27}Al assignments. All previous publications have observed a single ^{71}Ga line from doped LLZO, though the characteristics of the site were quite different in some cases (Howard *et al*., 2012; Bernuy-Lopez *et al*., 2014; Rettenwander *et al*., 2014b). For instance, the corresponding NMR spectra of Rettenwander *et al*. (2014b), who investigated the complete solid solution of Ga-doped LLZO (with Ga contents up to 0.84 pfu), revealed a single site with a large chemical shift (δ_{iso} = 244(2) ppm), a small quadrupole interaction (C_Q = 4.0(2) MHz), and an EFG tensor that deviates from axial symmetry (η_Q = 0.46(3)). The corresponding spectra are shown in Fig. 7.

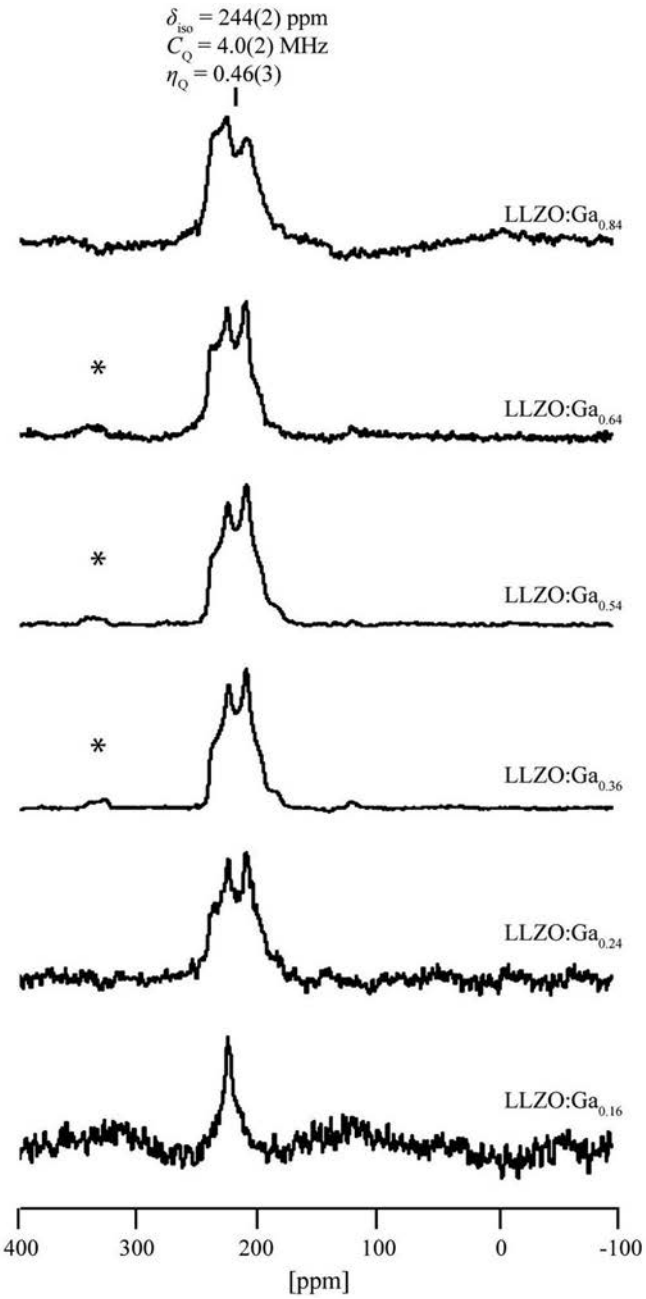

Fig. 7. The ^{71}Ga NMR spectra of $Li_{7-3x}Ga_xLa_3Zr_2O_{12}$ garnet with $0.16 < x < 0.84$ taken at 9.4 T (from Rettenwander *et al*. 2014b).

The study of Bernuy-Lopez *et al*. (2014), however, points to a Ga site with a smaller chemical shift (δ_{iso} = 207(10) ppm), a larger C_Q of 12.7(3) MHz, and an EFG tensor that is essentially axially symmetric (η_Q = 0.05(5)). These characteristics seem to mimic the two dopant sites in the ^{27}Al system discussed above, as would be expected for two elements in the same group of the periodic table.

It is therefore relatively straightforward to assign the higher chemical shift peak in the higher-field (21.1 T) spectra to Ga^{3+} ions located on the 96*h* site and the lower-chemical-shift peak to ions residing on the 24*d* site. This assignment is the only reasonable one provided that the local symmetry (–4) at the 24*d* site enforces axial symmetry on the EFG tensor (η_Q = 0). Local disorder, which slightly breaks this symmetry, probably varies somewhat with the preparation route; thus, some samples may display 24*d* site peaks that are better represented by a range of parameters rather than a single η = 0 site. Here, the signal of the 24*d* site can be best simulated with η_Q < 0.5 (see below).

The ^{71}Ga spectrum of the $Ga_{0.4}Al_{0.0}$ sample recorded at 21.1 T (Fig. 5) clearly shows both of the two sites that were observed individually in different samples. The signal at high chemical shift, δ_{iso} = 243(1) ppm, is narrow under the ultrahigh magnetic field applied, though an upper limit of 4.4 MHz can still be placed on C_Q. The lower-chemical-shift site, δ_{iso} = 193(1) ppm, is estimated to have a C_Q of 11.3(1) MHz and an upper limit of 0.5 can be placed on η using line shape simulations. These parameters are in close agreement with the published ^{71}Ga values and mimic the ^{27}Al NMR results as well; therefore, we assign the 243 ppm peak to the 96*h* site, and the 193 ppm peak to the 24*d* site.

It is quite interesting that three previous ^{71}Ga NMR studies of doped LLZO each reported that only one of the two sites was observed. Howard *et al*. (2012) and Rettenwander *et al.* (2014b) analysed Ga-doped LLZO at an applied field of 9.4 T with relatively slow sample spinning and observed only the narrow 96*h* line. On the other hand, Bernuy-Lopez *et al*. (2014) investigated LLZO doped with up to 0.30 pfu Ga at 11.75 T and fast sample spinning; they observed only the broad 24*d* signal. While the broad 96*h* signal may have been obscured by the lower magnetic field and slower spinning rates applied in the first two of these studies, there is little doubt that the narrow peak from the 96*h* site would easily have been observed in the study of Bernuy-Lopez *et al*. (2014) if Ga populated this site in the material. The observation of both sites in the same material presented here provides the first evidence that Ga can populate both the 96*h* and 24*d* sites in the same doped LLZO. This datum provides vital information on the structure and is important for developing the model of Li-ion dynamics in the system.

3.2.3 Site preferences of Al and Ga in dopant-stabilized LLZO

If we roughly assume that the area under the NMR line is proportional to the amount of the measured nuclei, the site distribution can be evaluated. The resulting site occupancies 24*d*: 96*h* are quite similar and range from 0.2: 0.1 (LLZO:$Ga_{0.0}Al_{0.4}$, LLZO:$Ga_{0.1}Al_{0.3}$) to 0.3: 0.1 (LLZO:$Ga_{0.2}Al_{0.2}$, LLZO:$Ga_{0.3}Al_{0.1}$, LLZO:$Ga_{0.4}Al_{0.0}$). Comparing the NMR spectra of the samples with a low amount of Ga incorporated (Fig. 4), there might be a tendency that at first the 96*h* position is preferentially occupied by Ga as compared to the 24*d* site. Considering the ^{27}Al MAS NMR spectrum of $Ga_{0.3}Al_{0.1}$ the Al^{3+} ions seem to prefer to occupy the 24*d* sites at first. Although we found a rather similar site preference for Al and Ga; the dopant distribution among the available sites in LLZO may of course strongly depend on the synthesis conditions chosen. This might also serve to explain differences in interpretation of Bernuy-Lopez *et al*. (2014) reporting that only the 24*d* site is occupied by Ga^{3+} ions.

4 Discussion

4.1 Phase stability and solubility of Fe

In this work we synthesized a series of LLZO:Fe_x with x_{obs} = 0.03 and x_{obs} = 0.25 Fe^{3+} pfu (x_{int} = 0.64 pfu). We were able to synthesize pure cubic LLZO with x_{obs} = 0.12(1) Fe^{3+} pfu and 6.54 Li pfu, whereby the former is the minimum amount of Fe^{3+} needed to obtain the pure cubic phase. The Li content of this garnet, *i.e*. 6.54 Li pfu, agrees with the reported Li content of 6.5 pfu that is necessary to stabilize the cubic modification of Ta- and Nb-doped LLZO (Thompson *et al*. 2014). Less Fe^{3+} (0.25 pfu) can be incorporated in LLZO compared to Al^{3+} (0.40 pfu) and Ga (about 0.70 pfu) under similar synthesis conditions (see below). This is possibly caused by increased Coulomb repulsion related to the higher degree of occupation of Fe^{3+} at 24*d* compared to the situation with Al^{3+} and Ga^{3+}.

The lattice constant a_0 = 12.980(5) Å in the various garnets does not vary significantly as a function of Fe^{3+} content. The substitution of 3 Li^+ ion with an ionic radius in tetrahedral coordination $r_{[4]}$ = 0.59 Å by 1 Fe^{3+} ion with $r_{[4]}$ = 0.49 Å has no big influence on the lattice constant a_0 of LLZO:Fe, in particular if we consider the low amounts of incorporated Fe. The XRPD results alone would seem to indicate an upper Fe^{3+} incorporation limit in LLZO of about x_{int} = 0.52. However, Fe^{3+} values in LLZO measured directly by electron microprobe are less than about x_{obs} = 0.25. It is also notable that phases other than LLZO were not observed in BSE images of samples with Fe contents up to x_{int} = 0.44, although $x_{obs} < x_{int}$. It appears that ^{57}Fe Mößbauer spectroscopy is more sensitive than XRPD in detecting small amounts of additional non garnet Fe-containing phases. The Mößbauer spectra of LLZO samples at Fe contents with $x_{int} \geq 0.24$ show that some possibly contain nano-crystalline $FeLaO_3$ occurring at grain boundaries of LLZO, where they are not easily detectable even by microprobe analysis.

4.2 Phase stability and solubility of Al and Ga

So far, efforts were spent to investigate the solubility of Al and Ga in LLZO and their influence on phase

behaviour. A detailed study on the role of the amount of Al and Li in cubic LLZO was presented by Rangasamy *et al*. (2012). The authors have shown that the Al content has to be above a critical concentration of 0.20 pfu to stabilize the cubic garnet phase. Otherwise, if the Al content is above 0.39 Al pfu two phases will form, cubic LLZO and $LaAlO_3$. Because Ga is located below Al in the periodic table one may suspect Ga to have similar effects on the stabilization of the cubic phase. Indeed, phase-pure cubic LLZO garnet can be obtained with a Ga content ranging from 0.16 to 0.72 Ga pfu (Rettenwander *et al.*, 2014b)

Rettenwander *et al*. (2015b) were able to show that mixed doping with Al and Ga stabilizes the cubic phase in the same way as known for doping with a single element. It turned out that the solubility of Ga is higher than that of Al. Furthermore, the amount of extra phases increases with increasing Al portion. Most likely, the reason for the lower incorporation limit of Al compared to Ga can be related to the larger difference between the radii of Li^+ ($r_{[4]} = 0.59$ Å; $r_{[6]} = 0.74$ Å) and Al^{3+} ($r_{[4]} = 0.39$ Å; $r_{[6]} = 0.53$ Å) compared to the difference between Li^+ and Ga^{3+} ($r_{[4]} = 0.47$ Å; $r_{[6]} = 0.62$ Å). According to Goldschmidt's rule the maximum change in ionic radii should be below approximately 15 % to fully substitute a given cation in solid solutions. Consequently, owing to the smaller radii of Al in different coordination spheres, one might expect a lower incorporation limit for Al^{3+} ions than for Ga^{3+} ions.

Apart from these studies, Düvel *et al*. (2012) reported on Al-doped LLZO samples with up to 1.76 Al pfu incorporated, namely $Li_{6.36}Al_{1.78}La_{2.27}Zr_{1.38}O_{12}$. Because of repulsive Li^+-Li^+ and Li^+-Al^{3+} interactions, not more than 60 out of 168 available Li sites per unit cell (= 7.5 Li pfu) can be occupied by Li that is distributed among the available sites 24*d*, 48*g* and 96*h*. This estimation is based on the assumption that, if a Li ion is located on a 24*d* site, Li ions in the direct neighbourhood will be displaced to a 96*h* void next to an empty 24*d* position. The value of 7.5 Li pfu is in agreement with the upper incorporation limit experimentally found by Rangasamy *et al*. (2012).

In our opinion, additional Al might also be found in side products such as $LiAlO_2$ or $LaAlO_3$ as mentioned above (Vosegaard *et al*., 1997). If present in an amorphous form, they are expected to be invisible by X-ray diffraction but detectable by NMR spectroscopy. Due to signal overlapping in ^{27}Al MAS NMR, however, it can be very difficult to detect such phases. As an example, δ_{iso} of crystalline or X-ray amorphous $LiAlO_2$ shows up at *ca*. 82 ppm which falls into the same ppm range of ^{27}Al on 96*h* in LLZO (Wohlmuth *et al.*, 2014) In Düvel *et al*. (2012) some of the ^{27}Al MAS NMR resonances at around 80 ppm, which should be interpreted as a single site in LLZO:Al, broaden with increasing Al content; a shoulder located at 82 ppm is visible for large Al portions. This feature might be attributed to the increasing formation of side products such as $LiAlO_2$. Extra phases may work as a sintering aid and assist in connecting the LLZO particles, thus enabling long-range ion transport because of reduced ion-blocking effects stemming from less conducting grain boundary regions. Note that, in analogy to the Al-doped oxides, the formation of crystalline $LiGaO_2$ has also been observed during the synthesis of Ga-bearing garnets (El Shinawi & Janek, 2013).

A possible influence of dopant cations on ionic mobility, *i.e.* conductivity, was first proposed by Allen *et al*. (2012). They discussed a possible blocking effect of dopants located at the Li-ion sub-lattice in garnets. Especially the 24*d* site might act as blockade for through-going ion diffusion as already noted above. Allen *et al*. (2012) investigated garnets of the composition $Li_{6.75}La_3Zr_{1.75}Ta_{0.25}O_{12}$ with and without doping using Al or Ga. At RT the undoped garnet showed the highest total Li-ion conductivity, $\sigma_{total} = 8.7 \times 10^{-4}$ S cm^{-1}. The corresponding activation energy, E_a, turned out to be 0.22 eV. These values were compared to the Al- and Ga-doped garnets being characterized by $\sigma_{total} = 3.7 \times 10^{-4}$ S cm^{-1} and 4.1×10^{-4} S cm^{-1} with $E_a = 0.30$ eV and 0.27 eV, respectively. The ionic conductivity of the pure $Li_{6.75}La_3Zr_{1.75}Ta_{0.25}O_{12}$ sample is reported to be twice that high compared to the samples doped with Ga and Al. The samples doped with Ga and Al showed similar electrochemical performances. The lattice parameter of the doped and undoped samples are reported to be $a_0 =$ 12.96 Å and $a_0 = 12.95$ Å respectively (Allen *et al*., 2012).

In our opinion, the increase of σ_{total} observed and the slight decrease of E_a found could also be related to the total amount of Li present or to the change in lattice constant a_0. Evidence for the latter is given by an earlier study of Murugan *et al*. (2008) who investigated the influence of the lattice parameter on ionic conductivity. The authors were able to show that the partial substitution of La^{3+} by divalent cations (*e.g.*, Ba^{2+}, Mg^{2+}, Ca^{2+}, Sr^{2+}) as well as by the use of higher sintering temperatures leads to an increase of a_0. This increase is accompanied by an increase of σ_{total} and a decrease of the E_a as well as an increasing grain boundary resistance R_{gb}. For example, $Li_6SrLa_2Ta_2O_{12}$ and $Li_6BaLa_2Ta_2O_{12}$ are characterized by $\sigma_{total} = 3.05 \times 10^{-5}$ S cm^{-1} and 9.28×10^{-5} S cm^{-1}, as well as $a_0 = 12.83$ Å and 12.97 Å, respectively. This means that an increase of 0.014 Å already leads to an increase of the ion conductivity by a factor of two; this is similar to what Allen *et al*. (2012) have observed.

Rettenwander *et al*. (2015b) found a decrease of the ^{7}Li line width (FWHM) as a function of the Ga content. Since the RT line width can be regarded as a qualitative measure of translational Li-ion dynamics, it means that the more Ga has been incorporated, the higher the Li-ion diffusivity. Because (i) the Li content remains constant and (ii) no significant site preference of the dopants Al and Ga was found, we tend to connect the increase in Li-ion dynamics, as seen by the change in Li NMR line widths, with the increase of a_0 rather than to the blocking effect of trivalent cations located on 24*d* sites.

The Li-ion conductivities of LLZO:Fe are not yet known. However, it should be mentioned that Li-ion conductivity measurement of single crystals of of

LLZO:Al, and LLZO:Ga, and LLZO:Fe are presently undertaken. These results will enable a direct comparison of the structure–ionic-conductivity relationships of LLZO:Al, LLZO:Ga, and LLZO:Fe.

Acknowledgements: The research was supported by Austrian Science Fund (FWF): project number P25702. Further support was by the Austrian Federal Ministry of Science, Research and Economy, and the Austrian National Foundation for Research, Technology and Development. M. W. and J. L. thank the DFG Research Unit 1277 for additional financial support.

References

Allen, J. L., Wolfenstine, J., Rangasamy, E., Sakamoto, J. (2012): Effect of substitution (Ta, Al, Ga) on the conductivity of $Li_7La_3Zr_2O_{12}$. *J. Power Sources*, 206, 315–319.

Amthauer, G., Annersten, H., Hafner, S. (1986): The Mößbauer spectrum of ^{57}Fe in silicate garnets. *Z. Kristallogr.*, 143, 14–55.

Awaka, J., Kijima, N., Hayakawa, H., Akimoto, J. (2009): Synthesis and structure analysis of tetragonal $Li_7La_3Zr_2O_{12}$. *J. Solid State Chem.*, 182, 2046–2052.

Bernuy-Lopez, C., Jr, Manalastas, Lopez, W, del Amo, J. M., Aguadero, A., Aguesse, F., Kilner, J. A. (2014): Atmosphere Controlled Processing of Ga-Substituted Garnets for High Li-Ion Conductivity Ceramics. *Chem. Mater.*, 26, 3610–3617.

Buschmann, H., Dölle, J., Berendts, S., Kuhn, A., Bottke, P., Wilkening, M., Heitjans, P., Senyshyn, A., Ehrenberg, H., Lotnyk, A., Duppel, V., Kienle, L., Janek, J. (2011): Structure and dynamics of the fast lithium ion conductor „$Li_7La_3Zr_2O_{12}$“. *Phys. Chem. Chem. Phys.*, 13, 19378–19392.

Cussen, E.J. (2010): Structure and ionic conductivity in lithium garnets. *J. Mat. Chem.*, 20, 5167–5173.

Düvel, A., Kuhn, A., Robben, L., Wilkening, M., Heitjans, P. (2012): Mechanosynthesis of solid electrolytes: Preparation, characterization, and Li ion transport of garnet-type Al-doped $Li_7La_3Zr_2O_{12}$ crystallizing with cubic symmetry. *J. Phys. Chem. C*, 116, 15192–15202.

El Shinawi, H., Janek, J. (2013): Stabilization of cubic lithium-stuffed garnets of the type “$Li_7La_3Zr_2O_{12}$“ by addition of gallium. *J. Power Sources*, 225, 13–19.

Geiger, C. A., Alekseev, E., Lazic, B., Fisch, M., Armbruster, T., Langner, R., Fechtelkord, M., Kim, N., Pettke, T., Weppner, W. (2011): Crystal chemistry and stability of „$Li_7La_3Zr_2O_{12}$“ garnet: a fast Li-ion conductor. *Inorg. Chem.*, 50, 1089–1097.

Han, J., Zhu, J., Li, Y., Yu, X., Wang, S., Wu, G., Xie, H., Vogel, S. C., Izumi, F., Momma, K., Kawamura, Y., Huang, Y., Goodenough, J.B., Zhao, Y. (2012): Experimental visualization of lithium conducting pathways in garnet-type $Li_7La_3Zr_2O_{12}$. *Chem. Commun.*, 48, 9840–9842.

Hellner, E., Gerlich, R., Koch, E., Fischer, W. (1979): The oxygen framework in garnet and its occurrence in the structures of $Na_3Al_2Li_3F_{12}$, $Ca_3Al_2(OH)_{12}$, $RhBi_4$, and Hg_3TeO_6. in “Physics Data“, H. Behrens & G. Ebel, eds. Fachinformationszentrum Energie, Physik, Mathematik, Karlsruhe, 16-1, 1–16.

Howard, M. A., Clemens, O., Kendrick, E., Knight, K. S., Apperly, P. A., Anderson, P. A., Slater, P. R. (2012): Effect of Ga incorporation on the structure and Li ion conductivity of $Li_7La_3Zr_2O_{12}$. *Dalton Trans.*, 41, 12048–12053.

Hubaud, A. A., Schroeder, D. J., Key, B., Ingram, B. J., Dogan, F., Vaughey, J. T. (2013): Low temperature stabilization of cubic $(Li_{7-3x}Al_x)La_3Zr_2O_{12}$: role of aluminum during formation. *J. Mater. Chem. A*, 1, 8813–8818.

Kuhn, A., Narayanan, S., Spencer, G., Goward, G., Thangadurai, V., Wilkening, M. (2011): Li self-diffusion in garnet-type $Li_7La_3Zr_2O_{12}$ as probed directly by diffusion-induced ^{7}Li spin-lattice relaxation NMR spectroscopy. *Phys. Rev. B*, 83, 094302–.

Lagarec, K., Rancourt, D. G. (1998): Extended Voigt-based analytic lineshape method for determining N-dimensional correlated hyperfine parameter distributions in Mößbauer spectroscopy. *Nucl. Instrum. Methods*, 129, 266–280.

Menzer, G. (1928): Die Kristallstruktur der Granate. *Z. Kristallogr*, 69, 300–396.

Murugan, R., Thangadurai, V., Weppner, W. (2007): Schnelle Lithium Ionenleitung in granatartigem $Li_7La_3Zr_2O_{12}$. *Angew. Chem.*, 119, 7925–7928.

Murugan, R., Thangadurai, V., Weppner, W. (2008): Lattice parameter and sintering temperature dependence of bulk and grain boundary conduction of garnet-like solid electrolytes. *J. Electrochem. Soc.*, 155, A90–A101.

Nitsche, R., Tippelt, G., Amthauer, G. (1994): Kinetics and thermodynamics of intercrystalline Fe- Ga-distribution in $Y_3(Fe, Ga)_5O_{12}$. *J. Mat. Sci*, 29, 2903–2910.

Ramzy, A., Thangadurai, V. (2010): Tailor-made development of fast Li ion conducting garnet-like solid electrolytes. *Appl. Mater. Interfaces*, 2, 385–390.

Rangasamy, E., Wolfenstine, J., Sakamoto, J. (2012): The role of Al and Li concentration on the formation of cubic garnet solid electrolyte of nominal composition $Li_7La_3Zr_2O_{12}$. *Solid State Ionics*, 206, 28–32.

Rettenwander, D., Geiger, C. A., Amthauer, G. (2013): Synthesis and Crystal Chemistry of the Fast Li-Ion Conductor $Li_7La_3Zr_2O_{12}$ Doped with Fe. *Inorg. Chem.*, 52, 8005–8009.

Rettenwander, D., Blaha, P., Laskowski, R., Schwarz, K., Bottke, P., Wilkening, M., Geiger, C. A., Amthauer, G. (2014a): DFT Study of the Role of Al^{3+} in the Fast Ion-Conductor $Li_{7-3x}Al^{3+}{}_xLa_3Zr_2O_{12}$ Garnet. *Chem. Mater.*, 26, 2617–2623.

Rettenwander, D., Geiger, C. A., Tribus, M., Tropper, P., Amthauer, G. (2014b): A Synthesis and Crystal Chemical Study of the Fast Ion Conductor $Li_{7-3x}Ga_xLa_3Zr_2O_{12}$ with □ = 0.08 to 0.84. *Inorg. Chem.*, 53, 6264–6269.

Rettenwander, D., Geiger, C.A., Tribus, M., Tropper, P., Wagner, R., Tippelt, G., Lottermoser, W., Amthauer, G. (2015a): The solubility and site preference of Fe in $Li_{7-3x}Fe_xLa_3Zr_2O_{12}$ garnets. *J. Solid State Chem.*, 230, 266–271.

Rettenwander, D., Langer, J., Walter Schmidt, W., Arrer, Ch., Harris, K.J., Terskikh, V., Goward, G.R., Wilkening, M., Amthauer, G. (2015b): Site occupation of Ga and Al in stabilized cubic $Li_{7-3(x+y)}Ga_xAl_yLa_3Zr_2O_{12}$ garnets as deduced from ^{27}Al and ^{71}Ga MAS NMR at ultrahigh magnetic fields. *Chem. Mater.*, 27, 3135–3142.

Shannon, R. D., Prewitt, C. T. (1969): Effective ionic radii in oxides and fluorides. *Acta Cryst.*, B 25, 925–946.

Sivakumar, M., Gedanken, A., Zhong, W., Jiang, Y. H., Du, Y. W., Brukental, I., Bhattacharya, D., Yeshurun, Y., Nowik, I. (2004):

Sonochemical synthesis of nanocrystalline $LaFeO_3$. *J. Mater. Chem.*, 14, 764–769.

Thangadurai, V., Narayanan, S., Pinzaru, D. (2014): Garnet-type solid-state fast Li ion conductors for Li batteries: critical review. *Chem. Soc. Rev.*, 43, 4714–4727.

Thompson, T., Wolfenstine, J., Allen, J. L., Johannes, M., Huq, A., David, I. N., Sakamoto, J. (2014): Tetragonal vs. cubic phase stability in Al-free Ta doped $Li_7La_3Zr_2O_{12}$ (LLZO. *J. Mat. Chem. A*, doi:10.1039/c4ta02099e

Vosegaard, T., Massiot, D., Gautier, N., Jakobsen, H. J. (1997): ^{71}Ga chemical shielding and quadrupole coupling tensors of the garnet $Y_3Ga_5O_{12}$ from single-crystal ^{71}Ga NMR. *Inorg. Chem.*, 36, 2446–2450.

Wohlmuth, D., Epp, V., Bottke, P., Hanzu, I., Bitschnau, B., Letofsky-Papst, I., Kriechbaum, M., Amenitsch, H., Hofer, F., Wilkening, M. (2014): Order vs. disorder-a huge increase in ionic conductivity of nanocrystalline $LiAlO_2$ embedded in an amorphous-like matrix of lithium aluminate. *J. Mater. Chem. A*, 2, 20295–20306.

Zeier, W. G. (2014): Structural limitations for optimizing garnet-type solid electrolytes: a perspective. *Dalton Trans.*, 43, 16133–16138.

Received 20 November 2015
Modified version received 27 February 2016
Accepted 24 March 2016